Supporting Information

Designing High-Performance Thermoelectrics through Chalcogen Engineering in InSe-based Layered Materials

Shivani Vinod[1], Tanu Choudhary[2], Raju K Biswas[1*]
[1]Department of Physics, North Eastern Regional Institute of Science and Technology, Nirjuli, Arunachal Pradesh 791109, India
[2]Department of Physics, Faculty of Natural Sciences, M S Ramaiah University of Applied Sciences, Bengaluru 560058, India
*E-mail: rajukumar1718@gmail.com

Table S1. Calculated lattice parameter, bond length, and bond angles of InSe, $InS_{0.5}Se_{0.5}$, $InS_{0.5}Te_{0.5}$ and $InSe_{0.5}Te_{0.5}$ estimated at PBE level.

Materials	**Lattice parameter (Å)**	**Bond length (Å)**	**Bond angle (deg)**
InSe	4.04	2.80 (In-In) 2.66 (In-Se)	98.53 (In-Se-In) 118.95 (In-In-Se)
$InS_{0.5}Se_{0.5}$	3.98	2.80 (In-In) 2.56 (In-S) 2.64(In-Se)	116.00 (In-In-S) 119.57 (In-In-Se) 102.22 (In-S-In) 97.73 (In-Se-In)
$InS_{0.5}Te_{0.5}$	4.15	2.79 (In-In) 2.61 (In-S) 2.81(In-Te)	113.12 (In-In-S) 121.57 (In-In-Te) 105.58 (In-S-In) 95.09 (In-Te-In)
$InSe_{0.5}Te_{0.5}$	4.24	2.80 (In-In) 2.71 (In-Se) 2.84 (In-Te)	115.57 (In-In-Se) 120.63 (In-In-Te) 102.73 (In-Se-In) 96.34 (In-Te-In)

Table S2. Energy separations between the highest and second-highest valence-band extrema (VB1–VB2), and the spacing between two conduction-band valleys (C_1–C_2) and valence-band valleys (V_1–V_2), for InSe, $InS_{0.5}Se_{0.5}$, $InS_{0.5}Te_{0.5}$ and $InSe_{0.5}Te_{0.5}$. These values quantify the degree of unconventional and conventional band convergence near the band edges, respectively.

	InSe	**$InS_{0.5}Se_{0.5}$**	**$InS_{0.5}Te_{0.5}$**	**$InSe_{0.5}Te_{0.5}$**
VB1-VB2 (eV)	0.61	0.60	0.54	0.55
C_1-C_2	0.71	0.70	0.74	0.73
V_1-V_2	0.28	0.30	0.37	0.26

Table S3. Calculated ICOHP and ICOBI value of InSe and its substituted systems estimated using LOBSTER code.

System	**Atomic pairs**	**ICOHP (eV)**	**ICOBI**
InSe	In-In	-3.89	0.79
	In-Se	-5.08	1.03
$InS_{0.5}Se_{0.5}$	In-In	-3.89	0.79
	In-Se	-5.19	1.03
	In-S	-5.24	0.99
$InS_{0.5}Te_{0.5}$	In-In	-3.87	0.80
	In-S	-4.90	0.97
	In-Te	-4.92	1.11
$InSe_{0.5}Te_{0.5}$	In-In	-3.86	0.81
	In-Se	-4.77	1.01
	In-Te	-4.76	1.10

Table S4. Calculated values of elastic constant (C_{3D}), deformation potential constant (E_1) effective mass (m^*), longitudinal acoustics phonon-limited carrier mobility (μ_{LA}), and relaxation time (τ_{LA}) calculated at 300K. ($m_0 = 9.1 \times 10^{-31}$ kg)

Material		**C_{3D} (10^{10} N/m)**	**E_1 (eV)**	**m^* (m_0)**	**μ_{LA} (cm^2/Vs)**	**τ_{LA} (10^{-12} s)**
InSe	**CB**	3.85	4.14	0.19	8247	0.89
	VB		1.47	0.59	3849	1.29
$InS_{0.5}Se_{0.5}$	**CB**	3.06	6.48	0.12	8440	0.57
	VB		4.16	0.56	435	0.13
$InS_{0.5}Te_{0.5}$	**CB**	3.68	1.21	0.18	105641	10.81
	VB		1.28	0.53	6345	1.91
$InSe_{0.5}Te_{0.5}$	**CB**	4.02	4.26	0.18	9310	0.9
	VB		4.47	0.51	625	0.18

Table S5. Calculated carrier concentration (n), mobility (μ) and electrical conductivity (σ) data for InSe-based bulk systems over a temperature range of 300 K to 600 K.

Temperature		InSe			$InS_{0.5}Se_{0.5}$			$InS_{0.5}Te_{0.5}$			$InSe_{0.5}Te_{0.5}$		
		n (cm^{-3}) 10^{16}	μ cm^2/Vs	σ S/cm	n (cm^{-3}) 10^{17}	μ cm^2/Vs	σ S/cm	n (cm^{-3}) 10^{18}	μ cm^2/Vs	σ S/cm	n (cm^{-3}) 10^{18}	μ cm^2/Vs	σ S/cm
300	**CB**	8	1995	25.54	3.0	1337	64.18	1.5	1506	361.4	2.0	1790	572.8
	VB		694	8.88		190	9.12		479	115.0		347	111.0
350	**CB**	10	1877	30.03	5.0	1284	102.7	1.8	1501	432.3	2.6	1705	709.3
	VB		663	10.61		171	13.68		470	135.4		303	126.0
400	**CB**	15	1765	42.36	6.0	1232	118.3	2.1	1495	502.3	3.4	1622	882.4
	VB		633	15.19		154	14.78		461	154.9		267	145.2
450	**CB**	20	1661	53.15	7.0	1181	132.3	2.4	1488	571.4	4.0	1542	986.9
	VB		603	19.30		139	15.57		451	173.2		237	151.7
500	**CB**	25	1561	62.44	8.0	1131	144.8	2.7	1482	640.2	4.6	1465	1078
	VB		575	23.00		126	16.13		441	190.5		211	155.3
550	**CB**	30	1469	70.51	9.0	1083	156.0	3.0	1475	708.0	5.4	1393	1204
	VB		548	26.30		115	16.56		431	206.9		190	164.2
600	**CB**	35	1383	77.45	10.0	1037	165.9	3.5	1468	822.1	6.0	1324	1271
	VB		522	29.23		105	17.0		421	235.8		172	165.1

Table S6. Calculated Seebeck coefficient (S), lattice thermal conductivity (κ_l), and electronic thermal conductivity (κ_e) data for InSe, $InS_{0.5}Se_{0.5}$, $InS_{0.5}Te_{0.5}$ and $InSe_{0.5}Te_{0.5}$ over a temperature range of 300 K to 600 K.

Temperature		InSe			$InS_{0.5}Se_{0.5}$			$InS_{0.5}Te_{0.5}$			$InSe_{0.5}Te_{0.5}$		
		S μV/K	κ_l W/mK	κ_e W/mK (10^{-5})	S μV/K	κ_l W/mK	κ_e W/mK (10^{-5})	S μV/K	κ_l W/mK	κ_e W/mK (10^{-4})	S μV/K	κ_l W/mK	κ_e W/mK (10^{-5})
300	**CB**	1014	1.71	18	753	3.59	47	448	2.47	265	375	2.00	421
	VB	933		6	862		7	556		84	476		81
350	**CB**	897	1.46	25	638	3.08	88	383	2.11	370	321	1.72	608
	VB	798		9	751		11	486		116	421		108
400	**CB**	805	1.28	41	555	2.70	115	337	1.84	492	284	1.52	864
	VB	701		14	666		14	434		151	383		142
450	**CB**	732	1.14	58	490	2.40	145	302	1.64	629	256	1.34	1088
	VB	619		21	602		17	393		190	351		167
500	**CB**	673	1.02	61	442	2.17	177	275	1.48	784	234	1.20	1320
	VB	557		28	548		19	364		233i	329		190
550	**CB**	621	0.93	95	402	1.97	210	255	1.34	954	215	1.09	1622
	VB	507		35	506		22	340		278	309		221
600	**CB**	585	0.85	113	369	1.81	243	235	1.23	1208	201	1.00	1868
	VB	466		42	473		24	319		346	292		242

Table S7. Calculated Specific heat (C_v) data for InSe, $InS_{0.5}Se_{0.5}$, $InS_{0.5}Te_{0.5}$ and $InSe_{0.5}Te_{0.5}$ over a temperature range of 300 K to 600 K.

C_v (10^6 J/m^{3}K)				
Temperature	**InSe**	**$InS_{0.5}Se_{0.5}$**	**$InS_{0.5}Te_{0.5}$**	**$InSe_{0.5}Te_{0.5}$**
300K	1.29	1.40	1.27	1.22
350K	1.30	1.42	1.28	1.23
400K	1.31	1.43	1.29	1.24
450K	1.32	1.44	1.30	1.24
500K	1.32	1.45	1.31	1.25
550K	1.33	1.46	1.31	1.25
600K	1.33	1.46	1.31	1.25

Table S8. Calculated power factor (PF) and figure of merit (ZT) data for InSe, $InS_{0.5}Se_{0.5}$, $InS_{0.5}Te_{0.5}$ and $InSe_{0.5}Te_{0.5}$ over a temperature range of 300 K to 600 K.

Temperature		InSe		$InS_{0.5}Se_{0.5}$		$InS_{0.5}Te_{0.5}$		$InSe_{0.5}Te_{0.5}$	
		PF(10^{-4})	ZT	PF(10^{-4})	ZT	PF(10^{-4})	ZT	PF(10^{-4})	ZT
300	**CB**	26.26	0.46	36.39	0.30	72.53	0.88	80.55	1.20
	VB	7.72	0.13	6.77	0.05	35.55	0.43	25.14	0.37
350	**CB**	24.16	0.58	41.80	0.47	63.41	1.05	73.08	1.48
	VB	6.75	0.16	7.71	0.08	31.98	0.53	22.33	0.45
400	**CB**	27.45	0.86	36.43	0.54	57.04	1.24	71.17	1.87
	VB	7.46	0.23	6.55	0.09	29.17	0.63	21.29	0.56
450	**CB**	28.47	1.12	31.76	0.59	52.11	1.43	64.67	2.17
	VB	7.39	0.29	5.64	0.10	26.75	0.73	18.68	0.62
500	**CB**	28.28	1.38	28.28	0.65	48.39	1.63	59.02	2.45
	VB	7.13	0.35	4.84	0.11	25.24	0.85	16.80	0.70
550	**CB**	27.19	1.61	25.21	0.70	35.84	1.88	55.65	2.80
	VB	6.76	0.39	42.39	0.12	23.91	0.98	15.67	0.79
600	**CB**	26.50	1.87	22.58	0.74	45.40	2.21	51.34	3.08
	VB	6.34	0.45	3.80	0.13	23.99	1.17	14.07	0.84

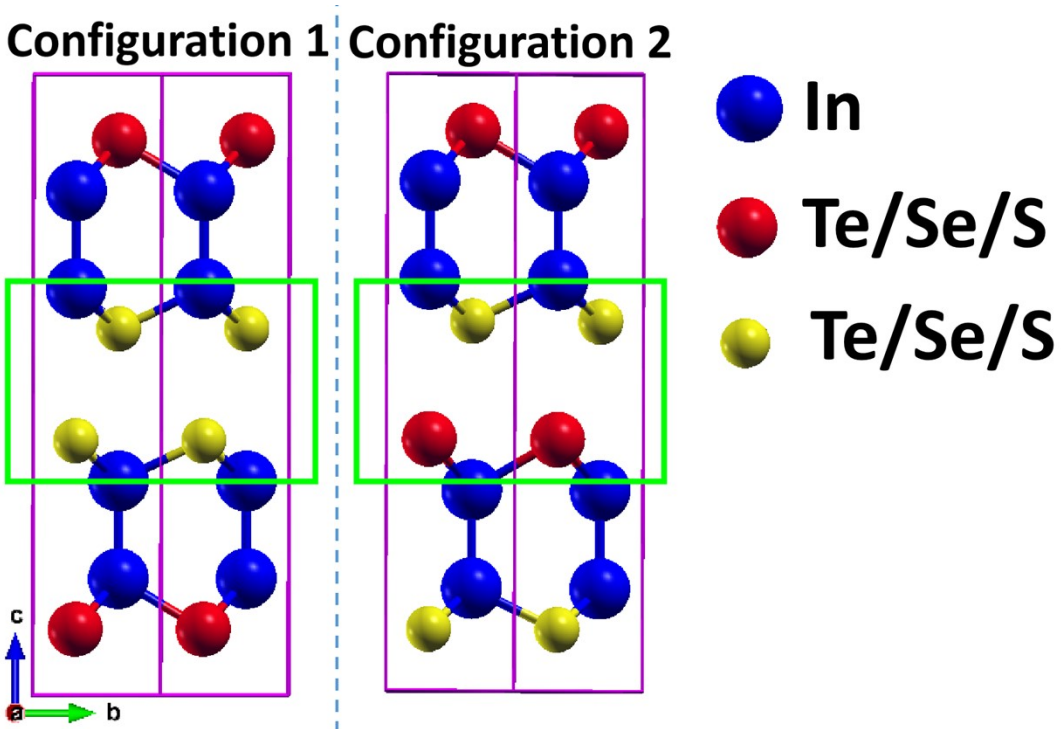

Fig. S1. Schematic illustration of the two possible stacking configurations of the chalcogen-substituted bulk structures. The green rectangular box highlights the interlayer van der Waals interface separating adjacent layers.

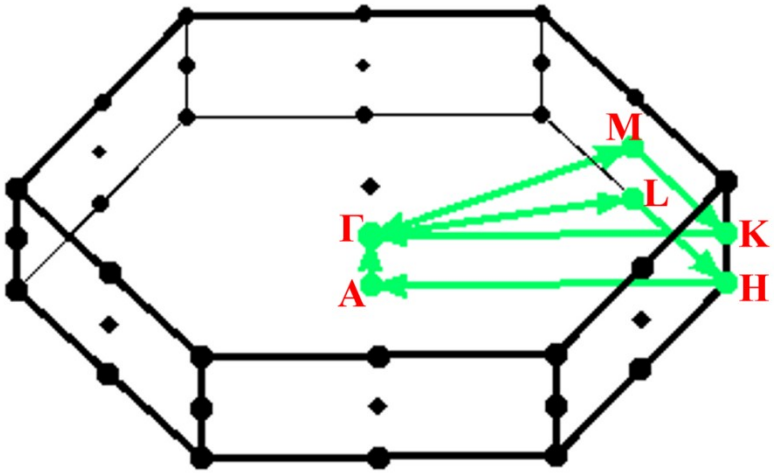

Fig. S2. Schematic representation of high symmetry points (Γ − M − K − Γ − L − H − A) in the hexagonal Brillouin zone (BZ) of all four systems.

Note S1

The strength of SOC is fundamentally governed by the atomic number Z of the constituent elements, scaling approximately as Z^4, such that heavier atoms are expected to exhibit progressively stronger relativistic effects [59, 60]. In the present InSe-based series, the substitution of Se by the lighter S atom (Z = 16) in $InS_{0.5}Se_{0.5}$ is expected to marginally reduce the overall SOC strength relative to pristine InSe (Se, Z = 34), whereas replacement by the heavier Te atom (Z = 52) in $InSe_{0.5}Te_{0.5}$ and $InS_{0.5}Te_{0.5}$ introduces a heavier chalcogen species that could in principle enhance relativistic contributions. However, despite this trend, the magnitude of SOC-induced changes remains uniformly small across all four compositions, with band-gap reductions not exceeding 0.01 eV in any system. This behavior is fully consistent with the fact that all constituent elements in these materials, namely Indium (Z = 49), Sulfur (Z = 16), Selenium (Z = 34), and Tellurium (Z = 52), belong to the p-block of the periodic table, for which spin–orbit interactions are governed primarily by intra-atomic p-orbital coupling.[84, 85] Although Te is substantially heavier than S and Se, its 5p orbitals participate in bonding interactions that partially delocalize the spin–orbit interaction across the lattice, reducing its localized impact on band-edge states. In contrast, compounds containing heavy d- or f-block elements, where SOC arises from strongly localized and energetically proximate d or f orbitals, typically exhibit far more pronounced relativistic band modifications, including large band splittings, significant band-gap renormalization, and substantial changes in band curvature.[84, 85] Since the electronic transport properties in the present systems depend primarily on band dispersion and carrier effective mass, both of which remain unaffected by SOC across the entire compositional series, spin–orbit coupling is excluded from all subsequent transport calculations without any loss of physical accuracy.

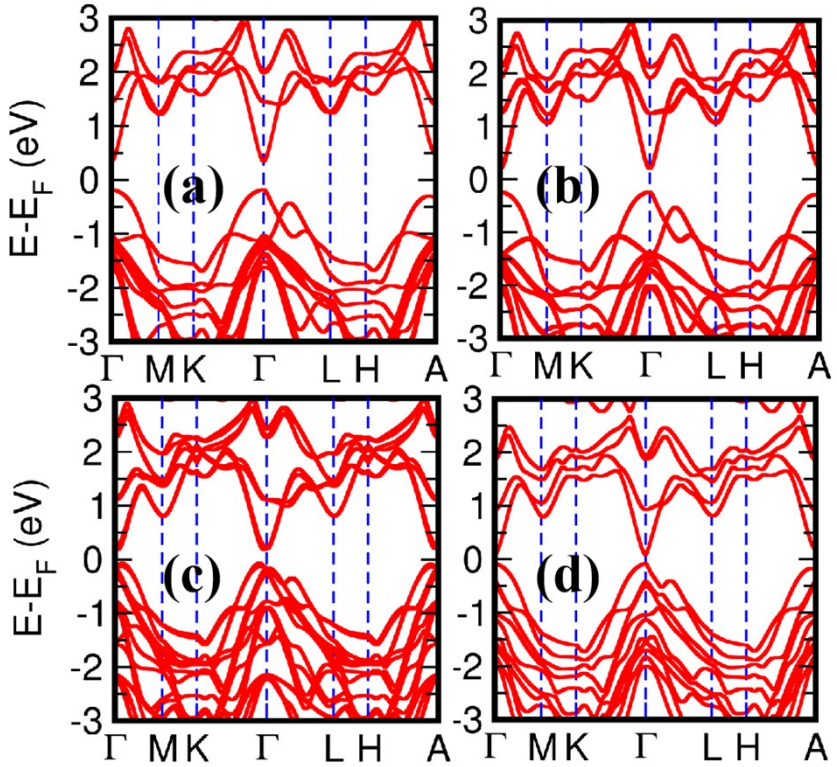

Fig. S3. Electronic band structure with SOC for (a) InSe, (b) $InS_{0.5}Se_{0.5}$, (c) $InS_{0.5}Te_{0.5}$ and (d) $InSe_{0.5}Te_{0.5}$, respectively.

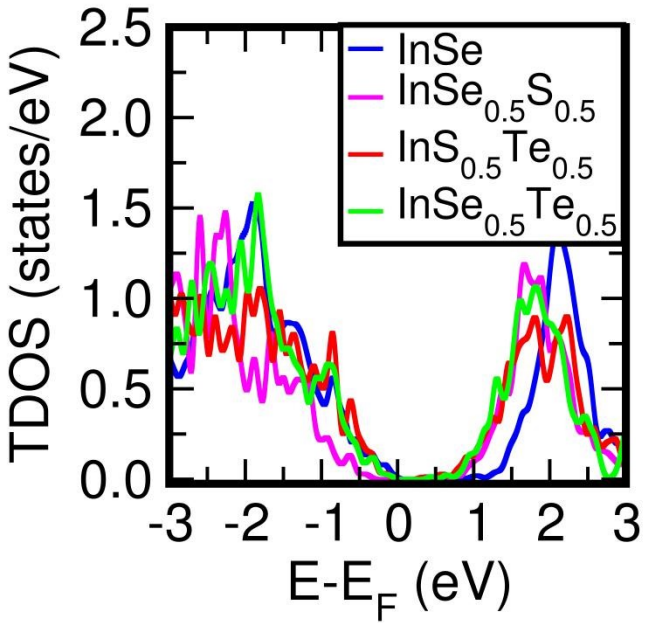

Fig. S4. Total density of states (TDOS) of InSe, $InS_{0.5}Se_{0.5}$, $InS_{0.5}Te_{0.5}$ and $InSe_{0.5}Te_{0.5}$.

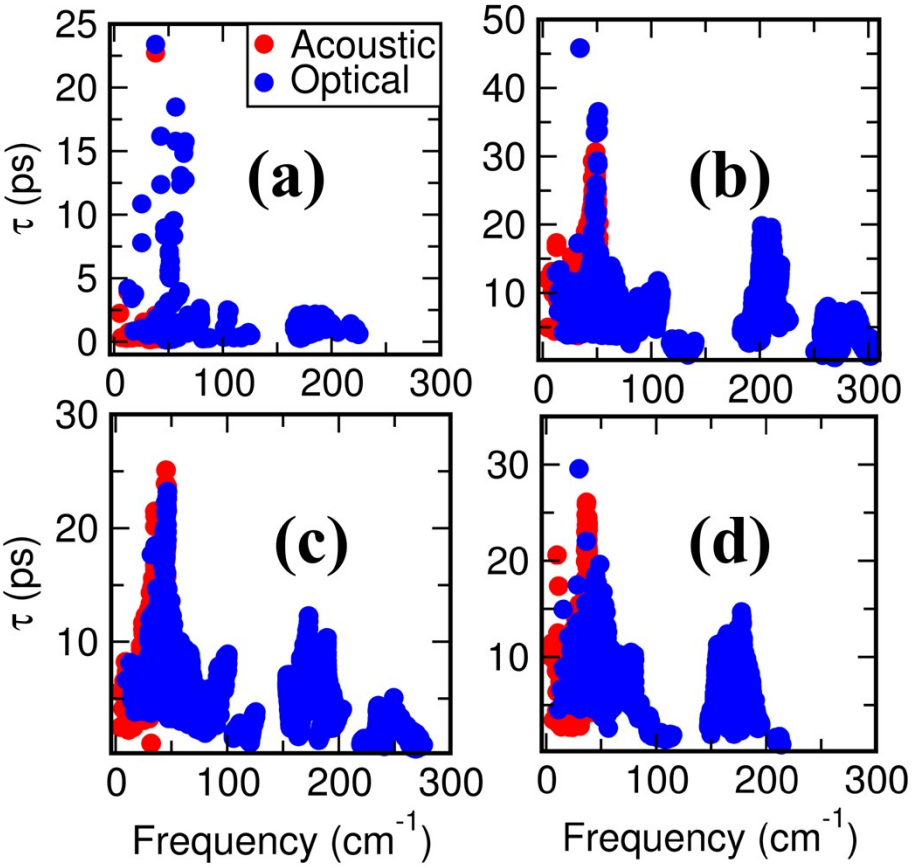

Fig. S5. Calculated phonon lifetime (τ) for (a) InSe, (b) $InS_{0.5}Se_{0.5}$, (c) $InS_{0.5}Te_{0.5}$ and (d) $InSe_{0.5}Te_{0.5}$, respectively.